# Biomimetic Submicroarrayed Cross-Linked Liquid Crystal Polymer Films with Different Wettability via Colloidal Lithography

Yuanyuan Zhan,[†] Jianqiang Zhao,[†] Wendong Liu,[‡] Bai Yang,[‡] Jia Wei,[†] and Yanlei Yu*,[†]

[†]Department of Materials Science & State Key Laboratory of Molecular Engineering of Polymers, Fudan University, Shanghai 200433, China

[‡]State Key Laboratory of Supramolecular Structure and Materials, College of Chemistry, Jilin University, Changchun 130012, China

Ⓢ Supporting Information

**ABSTRACT:** Photoresponsive cross-linked liquid crystal polymer (CLCP) films with different surface topographies, submicropillar arrays, and submicrocone arrays were fabricated through colloidal lithography technique by modulating different types of etching masks. The prepared submicropillar arrays were uniform with an average pillar diameter of 250 nm and the cone bottom diameter of the submicrocone arrays was about 400 nm, which are much smaller than previously reported CLCP micropillars. More interestingly, these two species of films with the same chemical structure represented completely different wetting behavior of water adhesion and mimicked rose petal and lotus leaf, respectively. Both the submicropillar arrayed film and the submicrocone arrayed film exhibited superhyrophobicity with a water contact angle (CA) value of 144.0 ± 1.7° and 156.4 ± 1.2°, respectively. Meanwhile, the former demonstrated a very high sliding angle (SA) greater than 90°, and thus, the water droplet was pinned on the surface as rose petal. On the contrary, the SA of the submicrocone arrayed CLCP film consisting of micro- and nanostructure was only 3.1 ± 2.0°, which is as low as that of lotus leaf. Furthermore, the change on the wettability of the films was also investigated under alternating irradiation of visible light with two different wavelengths, blue light and green light.

**KEYWORDS:** liquid crystal polymer, wettability, colloidal lithography, submicropillar, submicrocone
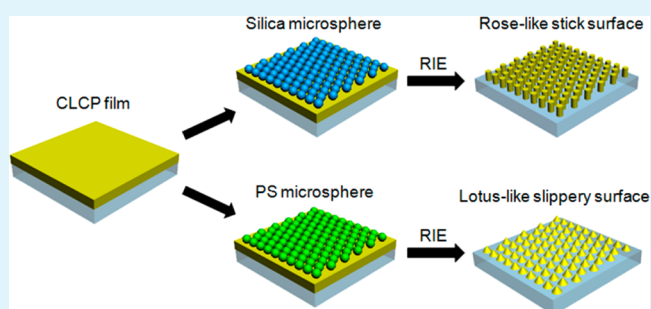
## INTRODUCTION

In nature, many biological materials exhibit unusual water repellency with aquatic high-loading and/or self-cleaning character, such as plant leaves,[1,2] insect wings,[3] water strider legs[4] and moths eyes.[5,6] Superhydrophobic properties with a contact angle (CA) higher than 150° originate from the combination of special micro/nano structures and low surface energy.[7–9] It is well-known that the roughness of protrusions leads to a reduced contact area between the surface and the water droplet. Thus, air is available to trap into microgrooves to form a cushion at the solid–liquid interface that prevents the solid from being wetted.[4] Inspired by this concept, liquid-repellent microtextured surfaces with liquid stickiness and nonstickiness have been widely studied.[10–15] The stick surface shows high surface adhesive force, and the water droplet can be pinned on the surface, while the nonstick surface allows the water droplet to easily roll off at a tilted angle less than 5° as a result of extremely low water adhesion. Because they have a range of potential applications, such as self-cleaning surfaces,[16] no-loss transport of microdroplet,[17] nonwetting liquid transfer,[18] and so on, various micro- and nanostructured surfaces with very high or very low water adhesion have been fabricated by modifying both surface roughness and composition.[19,20]

Consequently, fabrication of superhydrophobic bioinspired surfaces with controllable topography is desired. Formerly,

various techniques were applied to preparing microstructural surfaces, such as laser irradiation,[10] replica molding,[21] spin-coating,[8] nanoimprint lithography,[3] and etching techniques.[22–24] Among them, nanosphere lithography has been commonly used in recent years, for it is time-saving and can be modulated throughout etching procedure, which finely regulate the structural parameters such as shapes and dimensions.[23–25] Yang et al.[23] reported a colloidal lithography method using two-dimensional silica colloidal crystals as masks to fabricate ordered silicon cone arrays with controllable morphologies on a silicon substrate, and investigated their wettability in detail. Also, Jiang et al.[6] used spin-coated silica colloidal monolayer as etching mask to fabricate broadband antireflection coatings that mimic antireflective moth eyes. Recently, Yang et al.[25] presented a facile method to fabricate bioinspired polyethylene terephthalate nanocone arrays via colloidal lithography, and the sample exhibited underwater superoleophobicity with the underwater–oil CA of 171.8° and antibioadhension behavior. Most of these works emphasized hydrophobicity/hydrophilicity of surfaces achieved on different samples. Few of them involved a way of controlling water adhesion on superhydrophobic
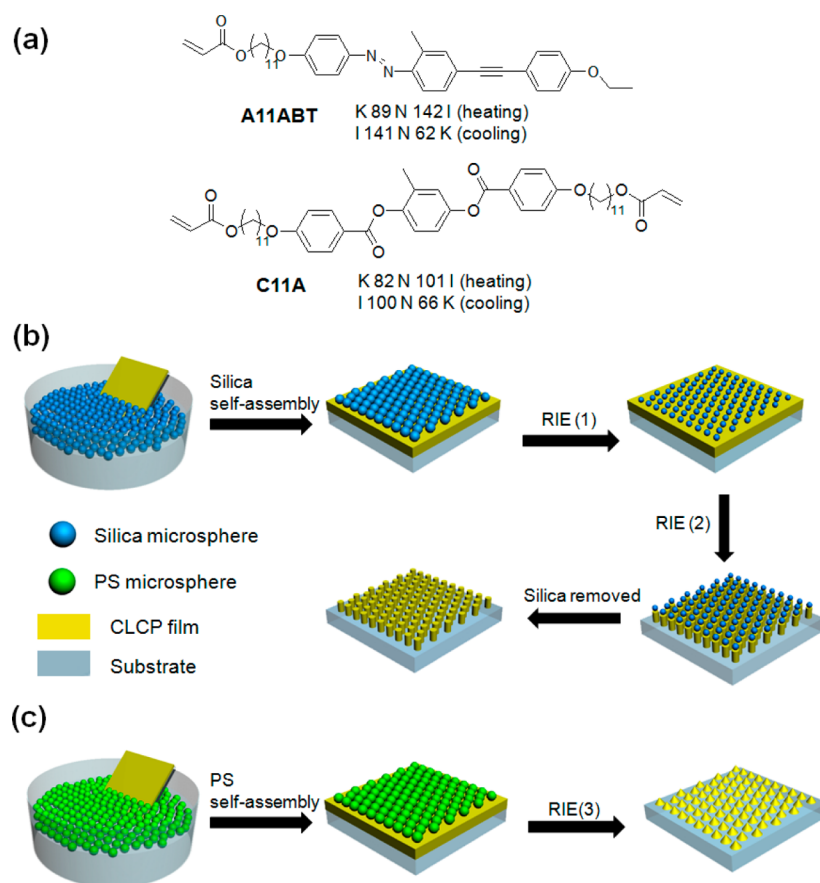
**Figure 1.** (a) Chemical structures and phase transition temperature of the LC monomers A11ABT and C11A. K, crystal; N, nematic; I, isotropic. (b and c) Schematic procedure of fabrication of microarrayed CLCP films. (b) Submicropillar arrayed CLCP film was obtained by four steps: First, silica microspheres were self-assembled on the surface of the cleaned CLCP films to prepare hcp 2D silica colloidal crystals monolayer via the modified interface method. Then, CLCP submicropillar arrays were prepared by the reactive ion etching (RIE) (1, 2) using a 7:3 mixture of CHCF3 and Ar as a process gas and oxygen gas, successively. Finally, the remained silica microspheres were removed by 1% HF solution. (c) Submicrocone arrayed CLCP film was obtained by two steps: First, PS microspheres were self-assembled on the surface of the cleaned CLCP film to form hcp 2D PS colloidal crystals monolayer via the modified interface method. Then, CLCP submicrocone arrays were obtained by a short time RIE (3) using 2D PS colloidal crystals as masks.

surface, which requires external stimuli to precisely manipulate surface composition.

To mimic the structure and function of biological systems, the search for smart materials that respond to external stimuli with shape or size change has attracted increasing attention.[26−28] Cross-linked liquid crystal polymers (CLCPs) appear as very promising candidates to build responsive surfaces because they possess such unique properties as elasticity, anisotropy, stimuli-responsiveness, and molecular cooperation effect.[29,30] The CLCPs, acted as actuators or artificial muscles,[31] can contract reversibly under various stimuli such as light[32,33] and temperature.[34−36] Conventionally, stimuli-responsive microactuators were fabricated from CLCPs using replica molding technique[27,34] and inkjet printing technology.[37] These CLCPs microactuators have greatly promoted the development of the field of surface-responsive surfaces where small geometric variations often lead to dramatic changes in surface properties, such as roughness and wettability. Keller et al. made micrometer sized thermal-actuated CLCP actuators using replica molding technique, which contracted reversibly by heating or cooling above their isotropic transition temperature.[27] Our group fabricated micrometer-scale arrayed CLCP films with superhydrophobic properties by polydimethylsiloxane-soft-template-based secondary replication.[21] Also, we used

replica molding technique to prepare a two-dimensional CLCP microarray with a period of about 1 $\mu$m.[32] The CLCP microarray showed switchable behavior on the reflection spectra under alternating irradiation of UV and visible light. However, there still remain many challenges in this filed. Above-mentioned microarrayed surfaces achieved with the CLCP pillars size of few micrometers were obtained by complex techniques. Moreover, few works focus on the fabrication of various types of surface morphologies and nanoscale structural arrays based on the CLCPs, which, however, play dominant roles in surface wettability.

Herein, we present two different surface topographies including submicropillar arrays and submicrocone arrays fabricated from azotolane-containing CLCP by using a time-efficient and high throughput etching technique of colloidal lithography. These two surfaces with different topographies exhibited superhyrophobicity and completely different wetting behavior of water adhesion, which can be easily obtained by modulating different types of etching masks throughout the fabrication process. The submicropillar arrayed film had a very high water sliding angle (SA) greater than 90°, whereas the submicrocone arrayed film exhibited an extremely low water SA of 3.1 ± 2.0°. Moreover, the submicropillar arrayed film still demonstrated the high water adhesion after blue light
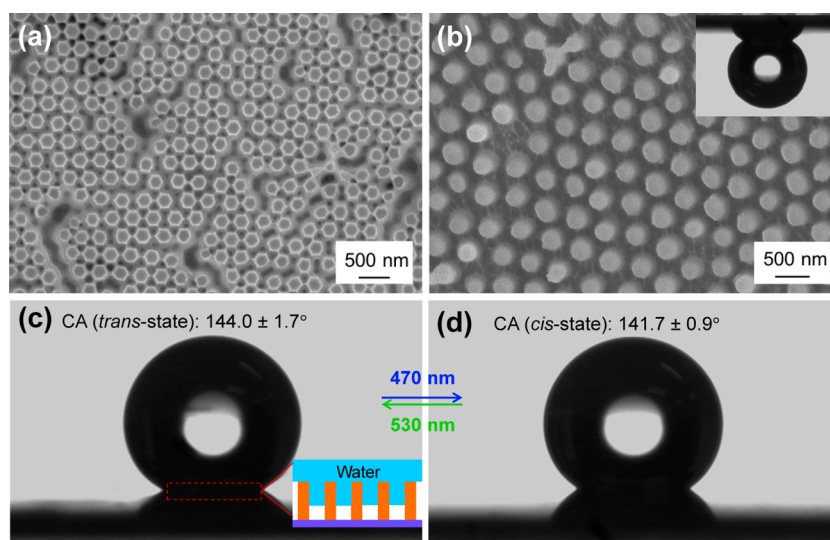
**Figure 2.** (a) Top view and (b) tilt angle view SEM images of submicropillar arrayed CLCP film. (b, inset) The shape of a water droplet on the CLCP film when it is turned upside down, indicating its high water adhesion. (c and d) Contacting behavior of a 5 $\mu$L water droplet on the submicropillar arrayed CLCP film in *trans*-state and *cis*-state, respectively. The surface after 470 nm light irradiation is in *cis*-state, and the average CA is 141.7 $\pm$ 0.9°, while the surface after 530 nm light irradiation is in *trans*-state, and the average CA is 144.0 $\pm$ 1.7°. The alternating irradiation time for blue light (470 nm, 120 mW cm$^{-2}$) and green light (530 nm, 30 mW cm$^{-2}$) was 120 s, respectively. (c, inset) Schematic of water intruding between the submicropillars.

irradiation, while SA of the submicrocone arrayed CLCP film after the blue light irradiation became twice as large as before. It is the first time to use the colloidal lithography technique to fabricate the CLCP films with submicro and even nanoscale structures, which have the same chemical structure but demonstrate different superhydrophobic adhesive properties to mimic rose petal and lotus leaf, respectively. These submicroarrayed CLCP films have potential applications as new smart surfaces with custom-tailored superhydrophobicity and water adhesion.

## ■ MATERIALS AND METHODS

**Materials.** The monomers used in this work include an azotolane monomer with a longer spacer (A11ABT) and a nonazotolane cross-linker with the undecyl spacer (C11A). The synthesis of A11ABT and C11A were carried out in a similar method which has been published.[38] The azotolane-containing CLCP films were prepared according to our previous work,[39,40] in which the mesogens were aligned parallel to the rubbing direction of polyimide due to the anchoring effect. The silica microsphere used in our work was 350 nm in diameter, purchased from Sphere Scientific Corporation. The polystyrene (PS) microsphere used was 1 $\mu$m in diameter, synthesized by the emulsion polymerization method.[41]

**Fabrication of Submicropillar Arrayed CLCP Film.** The CLCP submicropillar arrays were fabricated by colloidal lithography. First, the silica microspheres were dealt with hydrophobic surface treatment using trichloro(1H,1H,2H,2H-perfluorooctyl)silane. Then silica microspheres were self-assembled on the surface of the cleaned CLCP films to prepare hexagonal-close-packed (hcp) 2D silica colloidal crystals monolayer via the modified interface method.[42] Subsequently, the CLCP submicropillar arrays were prepared by reactive ion etching (RIE), using 2D silica colloidal crystals as masks by two steps. The RIE (1) process was performed using a 7:3 mixture of CHCF3 and Ar as a process gas at a total flow rate of 50 SCCM, chamber pressure 30 mTorr, RF power of 200 W, and ICP power of 0 W. Etching time was set to 3 min. The RIE (2) process was operated using 50 SCCM oxygen gas flow rate, chamber pressure 30 mTorr, RF power of 250 W, and ICP power of 50 W. Etching time was set to 20 min. The RIE was performed using Plasmalab 80 Plus (Oxford Instrument). After RIE, the remained silica microspheres were removed by 1% HF solution.

**Fabrication of Submicrocone Arrayed CLCP Film.** The fabrication procedures for the CLCP submicrocone arrays are similar to and shorter than that for the CLCP submicropillar arrays. First, the PS microspheres were self-assembled on the surface of the cleaned CLCP film to form hcp 2D PS colloidal crystals monolayer via the modified interface method. Then, CLCP submicrocone arrays were obtained by a short time RIE (3) using 2D PS colloidal crystals as masks. The RIE process operating at 50 SCCM oxygen gas flow rate, chamber pressure 30 mTorr, RF power of 250 W, and ICP power of 50 W was used for 12 min. The etching process went on until PS microspheres were etched off completely and thus the CLCP submicrocone arrays were obtained.

**Characterization.** The thermodynamic properties of the monomers, the mixtures and the azotolane-containing CLCP films were characterized by differential scanning calorimetry (DSC, TA Q2000) at the heating and cooling rates of 3 °C for the monomers and 10 °C for the films. Three scans operated to check the reproducibility. The mesomorphic properties of CLCP films were observed by polarizing optical microscope (POM, Leica 2500P) equipped with a Mettler hot stage (Mettler, model FP-90 and FP-82). Morphologies of the CLCP submicroarrays were observed by scanning electron microscopy (SEM) (JEOL FESEM 6700F Electron Microscope). Wettability of the azotolane films was investigated by CA and SA measurements on a contact angle system OCA15 (Contact Angle System OCA). The average CA and SA values were obtained by measuring the same submicroarrayed film at least in five different positions. The light intensities of the blue light-emitting diode (LED) (CCS, PJ-1505-2CA, HLV-24BL-3W, 470 nm) and the green-LED (CCS, PJ-1505-2CA, HLV-22GR-3W, 530 nm) for irradiation were 120 mW cm$^{-2}$ and 30 mW cm$^{-2}$, respectively.

## ■ RESULTS AND DISCUSSION

Figure 1a shows the chemical structures of azotolane-containing monomer (A11ABT) and nonazotolane cross-linker with the undecyl spacer (C11A). The microarrayed CLCP films composed of A11ABT and C11A are prepared by thermal polymerization of mixtures including the monomer and the cross-linker with a molar ratio of 1:9. Figure 1b,c represents the procedure for the fabrication of the submicropillar arrayed CLCP film and the submicrocone arrayed CLCP film,
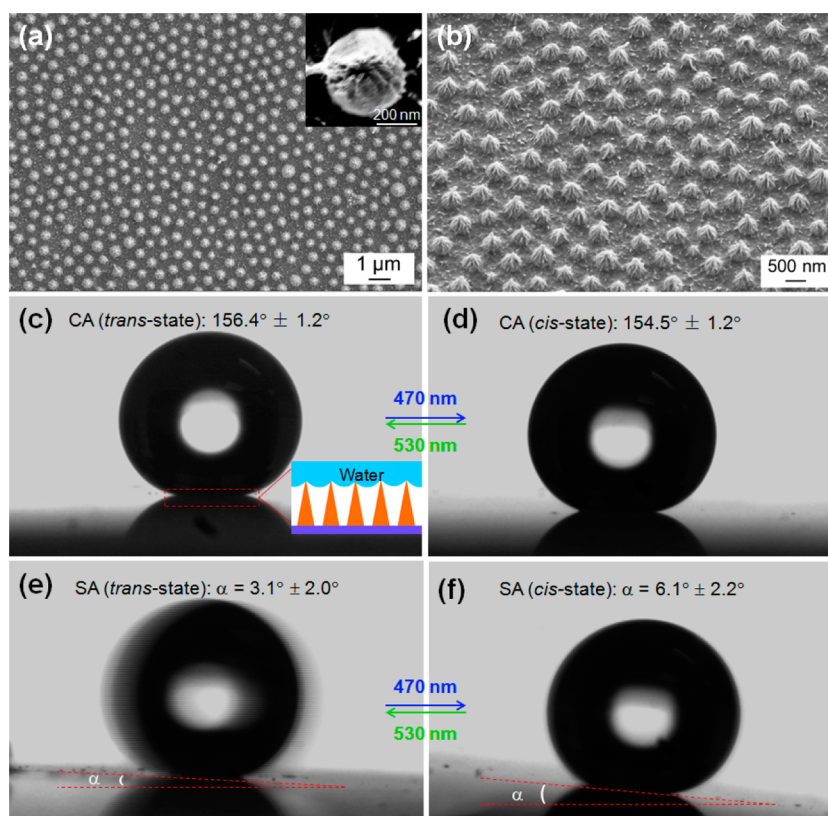
**Figure 3.** (a) Large area SEM image of the surface of submicrocone arrayed CLCP film (top view) and tilted-view (b). The inset in (a) shows enlarged view of a single submicrocone. (c and d) CA and (e and f) SA measurements of a 5 $\mu$L water droplet on submicrocone arrayed CLCP film in *trans*-state and *cis*-state, respectively. The surface after blue light irradiation is in *cis*-state, and the average CA and SA are 154.5 $\pm$ 1.2° and 6.1 $\pm$ 2.2°, respectively, while the surface after green light irradiation is in *trans*-state, and the average CA and SA are 156.4 $\pm$ 1.2° and 3.1 $\pm$ 2.0° respectively. (c, inset) Schematic of a water droplet riding on the extreme top portions of the submicrocone arrayed CLCP film. The submicrocone arrays were alternately irradiated by blue light (470 nm, 120 mW cm$^{-2}$) and green light (530 nm, 30 mW cm$^{-2}$) for 120 s, respectively.

respectively. We designed these two kinds of microarrayed films based on the following three aspects: (1) the azotolane-containing film can respond to visible light, resulting in surface polarity change and shape deformation due to photoisomerization and an enlarged conjugation structure of the azotolane moieties,[43] (2) the spacers with 11 methylenes in both monomer and cross-linker make the film more hydrophobic; and (3) instead of UV light, visible light is a more suitable stimulating source due to considerations of environmental friendliness and harmlessness to human health.

**Topography and Wetting Behavior of the Submicropillar Arrayed CLCP Film.** The SEM photographs of the submicropillar arrayed CLCP film on the glass substrate are shown in Figure 2a,b. It can be seen that submicropillars exhibit hexagonal nonclose-packed arrays vertical to the glass substrate over a large area (Figure 2a). These images demonstrate that the submicropillar arrays are uniform with an average diameter of sub-250 nm and an aspect ratio of 8. Although there exist some lines and point defects in self-assembled silica microspheres lifted up to the CLCP substrate of 2 cm$^2$, the silica microspheres account for almost 99% of the area, and this guarantees the homogeneous distribution of the submicropillar arrays (Figure S1). The submicropillar arrayed CLCP film exhibited enhanced hydrophobicity with a water CA value of 144.0 $\pm$ 1.7°; while the flat CLCP film exhibited only hydrophobicity with a CA of 116.1 $\pm$ 2.0° (Figure S2). Importantly, SA in both *trans* and *cis* states were greater than 90°, that is, a water droplet on the surface of the submicropillar

arrayed CLCP film was sphere in shape, which did not roll off even when the film was turned upside down (Figure 2b inset). These results demonstrate the submicropillar arrayed CLCP film provides a sufficient roughness for superhydrophobicity and yet high adhesive force with water on the surface, similar to the rose petal effect.

As Figure 2c,d shows, the water CA of 141.7 $\pm$ 0.9° in *cis*-configuration is lower than that in *trans*-configuration (144.0 $\pm$ 1.7°), which is in accordance with the *trans* to *cis* configuration transition induced by blue light, because of the higher local polarity in *cis* configuration. Subsequently, the azotolane mesogens return to a *trans* configuration, and the surface reverts to the higher CA after 530 nm light irradiation for 120 s. The CAs of the submicropillar arrayed CLCP film have no distinct difference before and after the blue light irradiation. Compared with UV light at 365 nm, when the CLCP films are irradiated by blue light with a longer wavelength of 470 nm, azotolane mesogens are difficult to undergo *trans* to *cis* photoisomerization because the available photons energy of the blue light to induce the photoisomerization decreases due to the lower absorption coefficient of the azotolane moieties at 470 nm than at 360 nm.

Figure 2b, inset, shows the shape of a water droplet on the CLCP film when it is turned upside down, indicating its high water adhesion. We believe that the trapped air in submicrogrooves between pillars form a cushion at the film-water interface (Figure 2c, inset).[44] Thus, when the water droplet is drawn on the surface, the volume change of trapped

air induces the negative pressure and generates high adhesive force. Even after the blue light irradiation, the submicropillar arrayed film kept the high water adhesion.

**Topography and Wetting Behavior of the Submicrocone Arrayed CLCP Film.** Naturally, lotus leaf is well-known for its superhydrophobicity owing to micro- and nanostructures together with hydrophobic epicuticular wax secreted on the surface. On the basis of this study, we designed a unique lotus-like superhydrophobic submicrocone arrayed CLCP film, with the value of CA as high as 156.4 ± 1.2° and a low SA of 3.1 ± 2.0°, to remove the surface stickiness by avoiding formation of closed air pockets.[20] The assumed mode for this super-hydrophobicity is that the water droplet rides only on the extreme top portions of the submicrocone arrayed CLCP film, as shown in Figure 3c, inset. Figure 3a,b show the SEM images of the top view and the tilted-view of the lotus-like submicrocone arrayed CLCP film. The submicrocone with an aspect ratio of 3 is about 400 nm in bottom diameter. Figure S3 shows the SEM image of the self-assembled PS microspheres lift up to the CLCP substrate of 2 cm². The PS microspheres occupy more than 99% of the area though there are some lines and point defects involved, which leads to ordered submicrocone arrays.

It is clearly seen from inset in Figure 3a that the submicrocone possesses hierarchical structures created by nanostructures on microstructures, which is similar to those of the lotus leaf. As a result, the submicrocone arrayed CLCP film featured superhydrophobic antiadhesion to water. It has been reported that available air trapped in the microgroove of the surface is important for enlarging the CA and lowering the SA.[45] Compared with microgrooves among the submicropillar arrays, those between the submicrocone arrays are more sufficient to trap air. Additionally, the reason for the SA of the submicrocone arrayed CLCP film lower than 5° is discrete contact between the solid surface and liquid, which affects the shape, the contact length, and continuity of three-phase contact line. In general, an unstable contact line can generate in a lower energy barrier for advancing and receding of the water droplet, thus resulting in a small SA.

The difference of CA value with alternating blue and green irradiation is very small due to the decreased contact length (Figure 3c,d), while the SA value after the blue light irradiation is twice as much as that after the green light irradiation (Figure 3e,f). The SA change of the submicrocone arrayed film ranging from 3.1 ± 2.0° to 6.1 ± 2.2° is induced by the photoisomerization of the azotolane moieties from *trans* to *cis* states. Additionally, photodeformation is possible to generate in microarrays when the film is exposed to 470 nm light due to the photoinduced alignment change of LC mesogens.[32] The thermal photographs of the submicroarrayed CLCP films were also measured, as Figure S5 in the Supporting Information demonstrates. The temperature of the submicropillar CLCP film and the submicrocone CLCP film increased by less than 2 °C when irradiated by blue light of 120 mW cm⁻² for 120 s. This weak thermal effect cannot induce thermal deformation in the submicroarrays, since the nematic−isotropic phase transition temperature of the CLCP films is around 100 °C.

**Photoinduced Repeatable Wetting Behavior of the Submicroarrayed CLCP Films.** It can be seen from Figure 4 that the CAs of both microarrayed CLCP films are increased with the introduction of surface roughness, even high into the superhydrophobic region. The water adhesion on the submicrocone arrayed film is obviously smaller compared
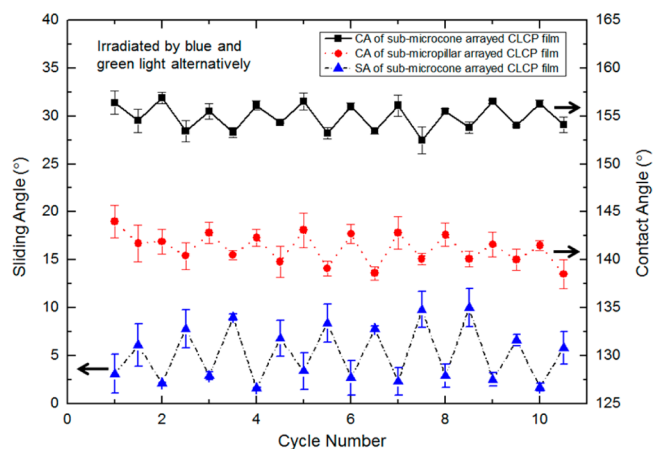


**Figure 4.** Ten cycles of CA and SA measurements with a 5 μL water droplet on the submicropillar arrayed CLCP film and the submicrocone arrayed CLCP film with alternating irradiation of blue light (470 nm, 120 mW cm⁻²) and green light (530 nm, 30 mW cm⁻²) for 120 s. The solid line and dash−dot line show the 10 cycles of CA and SA measurements of the submicrocone arrayed CLCP film, respectively. The dotted line shows the 10 cycles of CA measurement of the submicropillar arrayed CLCP film.

with the case of the flat film or the submicropillar arrayed film. We ascribe this to contact mode switching from Wenzel to Cassie mode with increasing surface roughness.[46] The shape change of the post from pillar to cone also leads to decreases in hysteresis due to the more contorted contact lines that form on these microarrayed films.[47] The CA increase from micropillar to microcone arrays is attributed to the decrease in the contact length and increase in tortuosity of the three-phase contact line.

Furthermore, reversible switching of CAs was induced well after 10 cycles in both microarrayed films under alternative irradiation of blue and green light. The lower CAs after blue light irradiation is due to photoisomerization of the azotolane mesogens from *trans*-state to *cis*-state, while the azotolane mesogens return to *trans*-state and both surfaces revert to higher CAs after green light irradiation. The submicropillar arrayed film kept the high water adhesion after the blue light irradiation, while the photoinduced reversible SA change of the submicrocone arrayed film was induced by alternating blue and green light irradiation. These results offer important information for designing controllable wettability with diverse surface topography.

## CONCLUSIONS

In conclusion, the submicropillar arrayed CLCP film and the submicrocone arrayed CLCP film with different wettability due to the controllable surface topography were fabricated using colloidal lithography technique. The microarrayed pillar and cone are uniform with average diameters of sub-250 nm and sub-400 nm, respectively, which are much smaller than ever reported. Owing to the surface chemistry and surface morphology designed to obtain substantial hydrophobicity, the submicropillar arrayed film exhibited hydrophobicity with high water adhesion similar to the case of rose petal, while the submicrocone arrayed film possessing a hierarchical morphology with dual length scale showed the water repellent characteristic, which can be favorably compared to that of the lotus leaf. Reversible CAs switching in superhydrophobic region was observed in both microarrayed films when alternately irradiated by blue and green light. Moreover, the submicropillar

arrayed film still demonstrated the high water adhesion after the blue light irradiation, while the photoinduced reversible SA change of the submicrocone arrayed film ranging between 3.1 ± 2.0° and 6.1 ± 2.2° was induced by alternating blue and green light irradiation. We believe that such a colloidal lithography method, in conjunction with CLCP, can be implemented to produce various types of surface topographies with further dynamic surface wettability just by regulating the etching masks throughout the fabrication process. It is anticipated that different surface topographies reported here may develop new promising applications of the CLCPs, especially in microfluidic devices, self-cleaning windows, and some other fields beyond the reach of current technologies.

## ■ ASSOCIATED CONTENT

### Ⓢ Supporting Information

The Supporting Information is available free of charge on the ACS Publications website at DOI: 10.1021/acsami.5b09013.

> The SEM images of silica microspheres self-assembled on the CLCP substrate, the flat CLCP film exhibiting hydrophobicity and the self-assembled PS microspheres (about 1 μm in diameter) over a large area, and tilt view SEM images of the submicropillar array and the submicrocone array, as well as thermal photographs of the submicroarrayed CLCP films. (PDF)

## ■ AUTHOR INFORMATION

### Corresponding Author
*E-mail: ylyu@fudan.edu.cn.

### Author Contributions

The manuscript was written through contributions of all authors. All authors have given approval to the final version of the manuscript.

### Notes

The authors declare no competing financial interest.

## ■ ACKNOWLEDGMENTS

## ■ REFERENCES

(1) Feng, L.; Li, S. H.; Li, Y. S.; Li, H. J.; Zhang, L. J.; Zhai, J.; Song, Y. L.; Liu, B. Q.; Jiang, L.; Zhu, D. B. Super-Hydrophobic Surfaces: From Natural to Artificial. *Adv. Mater.* **2002**, *14*, 1857−1860.

(2) Feng, L.; Zhang, Y. A.; Xi, J. M.; Zhu, Y.; Wang, N.; Xia, F.; Jiang, L. Petal Effect: A Superhydrophobic State with High Adhesive Force. *Langmuir* **2008**, *24*, 4114−4119.

(3) Zhang, G. M.; Zhang, J.; Xie, G. Y.; Liu, Z. F.; Shao, H. B. Cicada Wings: A Stamp from Nature for Nanoimprint Lithography. *Small* **2006**, *2*, 1440−1443.

(4) Gao, X. F.; Jiang, L. Water-Repellent Legs of Water Striders. *Nature* **2004**, *432*, 36−36.

(5) Stavenga, D. G.; Foletti, S.; Palasantzas, G.; Arikawa, K. Light on the Moth-Eye Corneal Nipple Array of Butterflies. *Proc. R. Soc. London, Ser. B* **2006**, *273*, 661−667.

(6) Sun, C. H.; Jiang, P.; Jiang, B. Broadband Moth-Eye Antireflection Coatings on Silicon. *Appl. Phys. Lett.* **2008**, *92*, 061112.

(7) Zhan, Y. Y.; Liu, Y. Y.; Lv, J. A.; Zhao, Y.; Yu, Y. L. Photoresponsive Surfaces with Controllable Wettability. *Prog. Chem.* **2015**, *27*, 157−167.

(8) Li, C.; Zhang, Y. Y.; Ju, J.; Cheng, F. T.; Liu, M. J.; Jiang, L.; Yu, Y. L. In Situ Fully Light-Driven Switching of Superhydrophobic Adhesion. *Adv. Funct. Mater.* **2012**, *22*, 760−763.

(9) Li, C.; Guo, R. W.; Jiang, X.; Hu, S. X.; Li, L.; Cao, X. Y.; Yang, H.; Song, Y. L.; Ma, Y. M.; Jiang, L. Reversible Switching of Water-Droplet Mobility on a Superhydrophobic Surface Based on a Phase Transition of a Side-Chain Liquid-Crystal Polymer. *Adv. Mater.* **2009**, *21*, 4254−4258.

(10) Zorba, V.; Stratakis, E.; Barberoglou, M.; Spanakis, E.; Tzanetakis, P.; Anastasiadis, S. H.; Fotakis, C. Biomimetic Artificial Surfaces Quantitatively Reproduce the Water Repellency of a Lotus Leaf. *Adv. Mater.* **2008**, *20*, 4049−4054.

(11) Wu, D.; Wang, J. N.; Wu, S. Z.; Chen, Q. D.; Zhao, S. A.; Zhang, H.; Sun, H. B.; Jiang, L. Three-Level Biomimetic Rice-Leaf Surfaces with Controllable Anisotropic Sliding. *Adv. Funct. Mater.* **2011**, *21*, 2927−2932.

(12) Yao, T. J.; Wang, C. X.; Lin, Q.; Li, X.; Chen, X. L.; Wu, J.; Zhang, J. H.; Yu, K.; Yang, B. Fabrication of Flexible Super-hydrophobic Films by Lift-Up Soft-Lithography and Decoration with Ag Nanoparticles. *Nanotechnology* **2009**, *20*, 065304.

(13) Wong, T. S.; Kang, S. H.; Tang, S. K. Y.; Smythe, E. J.; Hatton, B. D.; Grinthal, A.; Aizenberg, J. Bioinspired Self-Repairing Slippery Surfaces with Pressure-Stable Omniphobicity. *Nature* **2011**, *477*, 443−447.

(14) Dorrer, C.; Ruhe, J. Mimicking the Stenocara Beetle-Dewetting of Drops from a Patterned Superhydrophobic Surface. *Langmuir* **2008**, *24*, 6154−6158.

(15) Jiang, W. H.; Wang, G. J.; He, Y. N.; Wang, X. G.; An, Y. L.; Song, Y. L.; Jiang, L. Photo-Switched Wettability on an Electrostatic Self-Assembly Azobenzene Monolayer. *Chem. Commun.* **2005**, 3550−3552.

(16) Thiele, U.; Knobloch, E. Driven Drops on Heterogeneous Substrates: Onset of Sliding Motion. *Phys. Rev. Lett.* **2006**, *97*.10.1103/PhysRevLett.97.204501

(17) Hong, X.; Gao, X. F.; Jiang, L. Application of Superhydrophobic Surface with High Adhesive Force in No Lost Transport of Superparamagnetic Microdroplet. *J. Am. Chem. Soc.* **2007**, *129*, 1478−1479.

(18) Hou, X.; Hu, Y. H.; Grinthal, A.; Khan, M.; Aizenberg, J. Liquid-Based Gating Mechanism with Tunable Multiphase Selectivity and Antifouling Behaviour. *Nature* **2015**, *519*, 70−73.

(19) Bormashenko, E.; Stein, T.; Pogreb, R.; Aurbach, D. ″Petal Effect″ on Surfaces Based on Lycopodium: High-Stick Surfaces Demonstrating High Apparent Contact Angles. *J. Phys. Chem. C* **2009**, *113*, 5568−5572.

(20) Lai, Y. K.; Gao, X. F.; Zhuang, H. F.; Huang, J. Y.; Lin, C. J.; Jiang, L. Designing Superhydrophobic Porous Nanostructures with Tunable Water Adhesion. *Adv. Mater.* **2009**, *21*, 3799−3803.

(21) Li, C.; Cheng, F. T.; Lv, J. A.; Zhao, Y.; Liu, M. J.; Jiang, L.; Yu, Y. L. Light-Controlled Quick Switch of Adhesion on a Micro-Arrayed Liquid Crystal Polymer Superhydrophobic Film. *Soft Matter* **2012**, *8*, 3730−3733.

(22) Liu, W. D.; Li, Y. F.; Wang, T. Q.; Li, D. W.; Fang, L. P.; Zhu, S. J.; Shen, H. Z.; Zhang, J. H.; Sun, H. C.; Yang, B. Elliptical Polymer Brush Ring Array Mediated Protein Patterning and Cell Adhesion on Patterned Protein Surfaces. *ACS Appl. Mater. Interfaces* **2013**, *5*, 12587−12593.

(23) Zhang, X. M.; Zhang, J. H.; Ren, Z. Y.; Li, X.; Zhang, X.; Zhu, D. F.; Wang, T. Q.; Tian, T.; Yang, B. Morphology and Wettability Control of Silicon Cone Arrays Using Colloidal Lithography. *Langmuir* **2009**, *25*, 7375−7382.

(24) Li, Y. F.; Zhang, J. H.; Fang, L. P.; Wang, T. Q.; Zhu, S. J.; Li, Y.; Wang, Z. H.; Zhang, L.; Cui, L. Y.; Yang, B. Fabrication of Silicon/Polymer Composite Nanopost Arrays and Their Sensing Applications. *Small* **2011**, *7*, 2769−2774.

(25) Liu, W. D.; Liu, X. Y.; Fangteng, J. Z.; Wang, S. L.; Fang, L. P.; Shen, H. Z.; Xiang, S. Y.; Sun, H. C.; Yang, B. Bioinspired Polyethylene Terephthalate Nanocone Arrays with Underwater

Superoleophobicity and Anti-Bioadhesion Properties. *Nanoscale* **2014**, 6, 13845−13853.

(26) Wu, Z. L.; Buguin, A.; Yang, H.; Taulemesse, J. M.; Le Moigne, N.; Bergeret, A.; Wang, X. G.; Keller, P. Microstructured Nematic Liquid Crystalline Elastomer Surfaces with Switchable Wetting Properties. *Adv. Funct. Mater.* **2013**, 23, 3070−3076.

(27) Yang, H.; Buguin, A.; Taulemesse, J. M.; Kaneko, K.; Mery, S.; Bergeret, A.; Keller, P. Micron-Sized Main-Chain Liquid Crystalline Elastomer Actuators with Ultralarge Amplitude Contractions. *J. Am. Chem. Soc.* **2009**, 131, 15000−15004.

(28) Liu, D. Q.; Broer, D. J. Self-Assembled Dynamic 3D Fingerprints in Liquid-Crystal Coatings Towards Controllable Friction and Adhesion. *Angew. Chem., Int. Ed.* **2014**, 53, 4542−4546.

(29) Warner, M. Isotropic-to-Cholesteric Transition in Liquid Crystal Elastomers. *Phys. Rev. E: Stat. Phys., Plasmas, Fluids, Relat. Interdiscip. Top.* **2003**, 67.10.1103/PhysRevE.67.011701

(30) Yu, Y. L.; Maeda, T.; Mamiya, J.; Ikeda, T. Photomechanical Effects of Ferroelectric Liquid-Crystalline Elastomers Containing Azobenzene Chromophores. *Angew. Chem., Int. Ed.* **2007**, 46, 881−883.

(31) Jiang, H. R.; Li, C. S.; Huang, X. Z. Actuators Based on Liquid Crystalline Elastomer Materials. *Nanoscale* **2013**, 5, 5225−5240.

(32) Yan, Z.; Ji, X. M.; Wu, W.; Wei, J.; Yu, Y. L. Light-Switchable Behavior of a Microarray of Azobenzene Liquid Crystal Polymer Induced by Photodeformation. *Macromol. Rapid Commun.* **2012**, 33, 1362−1367.

(33) Wang, W.; Wang, X. Z.; Cheng, F. T.; Yu, Y. L.; Zhu, Y. T. Light-Driven Soft Actuators Based on Photoresponsive Polymer Materials. *Prog. Chem.* **2011**, 23, 1165−1173.

(34) Buguin, A.; Li, M. H.; Silberzan, P.; Ladoux, B.; Keller, P. Micro-actuators: When Artificial Muscles Made of Nematic Liquid Crystal Elastomers Meet Soft Lithography. *J. Am. Chem. Soc.* **2006**, 128, 1088−1089.

(35) Mol, G. N.; Harris, K. D.; Bastiaansen, C. W. M.; Broer, D. J. Thermo-Mechanical Responses of Liquid-Crystal Networks with a Splayed Molecular Organization. *Adv. Funct. Mater.* **2005**, 15, 1155−1159.

(36) Kuupfer, J.; Finkelmann, H. Liquid-Crystal Elastomers: Influence of the Orientational Distribution of the Cross-Links on the Phase-Behavior and Reorientation Processes. *Macromol. Chem. Phys.* **1994**, 195, 1353−1367.

(37) van Oosten, C. L.; Bastiaansen, C. W. M.; Broer, D. J. Printed Artificial Cilia from Liquid-Crystal Network Actuators Modularly Driven by Light. *Nat. Mater.* **2009**, 8, 677−682.

(38) Zhao, J. Q.; Yu, Y. L. Visible Light Induced Bending Behavior of Crosslinked Liquid Crystal Polymers Containing Azotolane with a Longer Spacer. *Mol. Cryst. Liq. Cryst.* **2014**, 601, 134−141.

(39) Wang, W.; Sun, X. M.; Wu, W.; Peng, H. S.; Yu, Y. L. Photoinduced Deformation of Crosslinked Liquid-Crystalline Polymer Film Oriented by a Highly Aligned Carbon Nanotube Sheet. *Angew. Chem., Int. Ed.* **2012**, 51, 4644−4647.

(40) Jiang, Z.; Xu, M.; Li, F. Y.; Yu, Y. L. Red-Light-Controllable Liquid-Crystal Soft Actuators via Low-Power Excited Upconversion Based on Triplet-Triplet Annihilation. *J. Am. Chem. Soc.* **2013**, 135, 16446−16453.

(41) Liu, J.; Chew, C. H.; Gan, L. M.; Teo, W. K.; Gan, L. H. Synthesis of Monodisperse Polystyrene Microlatexes by Emulsion Polymerization using a Polymerizable Surfactant. *Langmuir* **1997**, 13, 4988−4994.

(42) Rybczynski, J.; Ebels, U.; Giersig, M. Large-Scale, 2D Arrays of Magnetic Nanoparticles. *Colloids Surf., A* **2003**, 219, 1−6.

(43) Cheng, F. T.; Zhang, Y. Y.; Yin, R. Y.; Yu, Y. L. Visible Light Induced Bending and Unbending Behavior of Crosslinked Liquid-Crystalline Polymer Films Containing Azotolane Moieties. *J. Mater. Chem.* **2010**, 20, 4888−4896.

(44) Bico, J.; Tordeux, C.; Quere, D. Rough Wetting. *Europhys. Lett.* **2001**, 55, 214−220.

(45) Yoshimitsu, Z.; Nakajima, A.; Watanabe, T.; Hashimoto, K. Effects of Surface Structure on the Hydrophobicity and Sliding Behavior of Water Droplets. *Langmuir* **2002**, 18, 5818−5822.

(46) Furmidge, C. G. L. Studies at Phase Interfaces. I. The Sliding of Liquid Drops on Solid Surfaces and a Theory for Spray Retention. *J. Colloid Sci.* **1962**, 17, 309−324.

(47) Oner, D.; McCarthy, T. J. Ultrahydrophobic Surfaces. Effects of Topography Length Scales on Wettability. *Langmuir* **2000**, 16, 7777−7782.